Materials Today Bio 13 (2022) 100212

Contents lists available at ScienceDirect

Materials Today Bio

journal homepage: www.journals.elsevier.com/materials-today-bio

# The involvement of extracellular vesicles in the transcytosis of nanoliposomes through brain endothelial cells, and the impact of liposomal pH-sensitivity

Joy N. Reginald-Opara [a], Darren Svirskis [a], Song Yee Paek [b], Mingtan Tang [a], Simon J. O'Carroll [c], Justin M. Dean [d], Lawrence W. Chamley [b], Zimei Wu [a,*]

[a] School of Pharmacy, Faculty of Medical and Health Sciences, The University of Auckland, Auckland, 1142, New Zealand
[b] Hub for Extracellular Vesicles Investigations, Department of Obstetrics and Gynaecology, Faculty of Medical and Health Sciences, The University of Auckland, Auckland, 1142, New Zealand
[c] Department of Anatomy and Medical Imaging, Faculty of Medical and Health Sciences, The University of Auckland, Auckland, 1142, New Zealand
[d] Department of Physiology, Faculty of Medical and Health Sciences, The University of Auckland, Auckland, 1142, New Zealand

ARTICLE INFO

*Keywords:*
Blood brain barrier
Glutathione (GSH)-liposomes
pH-sensitivity
Human brain microvascular endothelial cells
Transcytosis
Endosome escape
Exocytosis
Extracellular vesicles

ABSTRACT

Despite the demonstrated effectiveness of nano-materials for drug delivery to the brain, a comprehensive understanding of their transport processes across the blood brain barrier (BBB) remains undefined. This multidisciplinary study aimed to gain an insight into the transport processes across BBB, focusing on the transcytosis of liposomes and the impact of liposomal pH-sensitivity. Glutathione-PEGylated pH-sensitive (GSH-PEG-pSL) and non pH-sensitive liposomes (GSH-PEG-L) were fluorescently labelled with rhodamine-DOPE and calcein, both impermeable to biomembranes. Following exposure to brain microvascular endothelial cells (hBMECs), the key functional component of the BBB, intracellular trafficking were evaluated by confocal live-cell imaging. The exocytosed liposomes, including naturally-occurring extracellular vesicles (EVs), were collected using differential centrifugation and and characterised regarding the EV yield, morphology and EVs origin using nanoparticle tracking analysis, transmission electron microscopy and flow cytometry. The transcytosis of liposomes through a verified BBB model comprising of hBMECs monolayer was also quantified. GSH-PEG-L was initially retained in the endo-lysosomes before exocytosed while packed in EVs of different sizes (<100 nm to >1 μm) while GSH-PEG-pSL underwent endosome escape with less degree of exocytosis with more fluorescence remaining in the cytoplasm. Compared with the untreated, hBMECs treated with GSH-PEG-L increased the yield of nano-EV and medium-EV by 7.9-fold and 4.6-fold, respectively. Conversely, GSH-pSL-treated cells produced 2.9-fold more nano-EVs but 2-fold less medium-EVs than the control cells. These vesicles were CD144-positive confirming their endothelial cell-origin. GSH-PEG-L demonstrated 2-fold higher efficiencies than GSH-PEG-pSL to cross the *in vitro* BBB model via exocytosis. Taken together, GSH-PEG-L might utilize EV secretion pathway to achieve transcytosis across brain endothelial cells of the BBB while liposomal pH-sensitivity favors cytoplasmic delivery.

## 1. Introduction

The highly restrictive nature of the blood brain barrier (BBB) necessitates novel 'transcellular mechanisms' to enhance drug delivery efficiency to the brain. Glutathione (GSH) modified-PEGylated liposomes (GSH-PEG-L) have been demonstrated to facilitate GSH-receptors-mediated brain delivery of various drugs [1–3], with efficiency proportional to GSH densities [4]. In addition, lipid composition [5] and other major factors, including size, surface charge, and drug release rate [6–8], has governed the brain-targeting efficiency.

Further advancement in recent years, include the use of pH-sensitive liposomes (pSL) to enhance the delivery of chemotherapeutic agents [9–12] to brain tumours [13–15] with advantages over the conventional (non pH-sensitive) liposomes [16]. Most pSLs are designed to be stable in neutral pH but destabilize in the acidic lumen of endosomes and lysosomes (collectively known as endo-lysosomes, pH 4.5–6.5) [17,18], releasing its contents into cytoplasm (endosome escape) [19–23]. The pSL containing 1,2-dioleoyl-sn-glycero-3-phosphoethanolamine (DOPE)

* Corresponding author.
*E-mail address:* z.wu@auckland.ac.nz (Z. Wu).

https://doi.org/10.1016/j.mtbio.2022.100212
Received 8 November 2021; Received in revised form 31 January 2022; Accepted 2 February 2022
Available online 5 February 2022

and cholesteryl hemisuccinate (CHEMS) could also enhance cellular uptake and endosome escape [19]. However, despite the mounting evidence for improved drug delivery efficiency with these strategies, the comprehensive knowledge of the transport processes of liposomes across the BBB is yet to be revealed.

In general, transport of materials across cells involves three major phases, endocytosis, endosomal sorting, and exocytosis [24,25], which is defined as 'transcytosis' [26,27]. As transcytosis is an active process, it can overcome the hindrance of the brain microvascular endothelial cells (BEC) of the BBB and provide a favourable transport pathway to brain. Many studies have focused on the endocytosis liposomes [4,28,29] and endosome escape mechanisms [30], with little or no specific studies unveiling the exocytosis mechanism [31]. Recent research has identified cellular mechanisms implicated in the transcytosis of polymeric and lipid-based nanoparticles through epithelial cell (keratinocytes and Caco-2) monolayers [32,33]. This suggested that internalised nanoparticles may be transported to the late endosomes or multivesicular bodies (MVB) and then to lysosomes for degradation or transported along a different pathway for exocytosis. Thus, we hypothesised that the internalised liposomes, which tend to remain in endosomes in BECs, can be incorporated into intralumenal vesicles of MVB and are subsequently extruded as extracellular vesicles (EVs). On the other hand, pSL may fuse with the endosomal membrane, releasing the payload in cytosol and subsequently impact the transcytosis efficiency via EV secretion.

EVs are a collective term describing vesicles of varying sizes released from various cell types including BECs [34–36], including small EVs (sEVs), medium and large EVs. sEVs previously referred to nano-EVs, and a subset of which is 'exosomes' have a diameter of less than 150 nm. Medium EVs (mEV), also referred to as micro-vesicles, have a size range from 150 to 1000 nm, while large EVs (such as apoptotic bodies) are >1000 nm in diameter [35,36]. Exosomes are produced via the endosomal pathway, while other sEVs and mEVs are formed by outward budding from the plasma membrane. BECs have been shown to release EVs that can be released into the blood and their specific biomarkers can reflect brain disorders [36]. Containing nuclear materials, lipids, and proteins of the parent cell, EVs are also crucial regulators of cell-cell communication by transferring content from parent cells to receipt cells [34,37].

To test our hypothesis, and gain insights into the transport mechanisms of liposomes through the BBB, in this work we examined the cellular trafficking of GSH-PEG-liposomes (as a model of ligand-modified liposomes) in brain microvascular endothelial cells, focusing on 'exocytosis'. We also aimed to investigate the effect of pH-sensitivity on the transcellular transport process of liposomes. The liposomal membrane was labelled with 1,2-dioleoyl-sn-glycero-3-phosphoethanolamine-N-(lissamine rhodamine B sulfonyl) (Rh-PE), and the aqueous cores with calcein (XLog P −3.1; MW 622.5). Both fluorescent probes were considered to be membrane-impermeable given their extremely high lipophilicity (Rh-PE) or hydrophilicity (calcein). Live-cell imaging technique [38,39] was employed to investigate the intracellular trafficking and exocytosis of both liposomes in human brain microvascular endothelial cells (hBMECs), the major functional component of BBB. To evaluate exocytosis, EVs released from the liposome-treated hBMECs were isolated using the standard differential centrifugation protocol for natural EVs. The mEVs and sEVs fractions expected to be liposome-EV hybrids were investigated regarding vesicle number, size, and morphology. Finally, the transport efficiency via this pathway was investigated using an *in vitro* hBMEC monolayer BBB model by measuring the Rh-PE in the 'brain side' compartment.

## 2. Materials and methods

### 2.1. Materials

The lipids, DOPE, CHEMS, 1,2-distearoyl-sn-glycero-3-phosphocholine (DSPC), 1,2-dipalmitoyl-sn-glycero-3-phosphocholine (DPPC), cholesterol, N-(carbonyl-methoxypolyethylenglycol2000)-1,2-dipalmitoyl-sn-glycero-3 phosphoethanolamine sodium (mPEG-DPPE2000), 1,2-distearoyl-sn-glycero-3-phosphoethanolamine-N-[maleimide (polyethylene glycol)-2000] ammonium salt (DSPE-PEG-maleimide) and 1,2-dioleoyl-sn-glycero-3-phosphoethanolamine-N-(lissamine rhodamine B sulfonyl) as ammonium salt (Rh-PE) were purchased from Sigma-Aldrich, Ltd. (Auckland, New Zealand). The hBMECs were purchased from Neurotics (Minneapolis, USA) at the first passage. The Cluster of Differentiation 144 (CD144), also known as the VE-cadherin (vascular endothelial cadherin) antibody, was purchased from Thermo Fisher Scientific (Auckland). Cell staining, immunofluorescence reagents, and other materials can be found in the electronic supplementary information.

### 2.2. Preparation and characterisation of GSH-PEG-liposomes

GSH-PEG-L and GSH-PEG-pSL with 4% GSH density were prepared by a direct GSH conjugation of preformed liposomes as described previously [40]. Briefly, liposomes containing DSPC:DOPE:CHEMS:cholesterol: mPEG-DPPE2000/DSPE-PEG2000 maleimide at molar ratios of 2:4:2:2:0.1:0.4 (for GSH-PEG-pSL) or DPPC/cholesterol/mPEG-DPPE 2000/DSPE-PEG2000 maleimide at 6:4:0.1:0.4 (for GSH-PEG-L) were prepared with thin-film hydration extrusion method before conjugation with free GSH.

To prepare fluorescent-labelled GSH-PEG-liposomes, Rh-PE (0.3 mg per 20 mg of lipids) was added in the lipid phase [39], while a 10 mM calcein in 10 mM HEPES buffer (pH 7.4) solution was used as the hydration medium.

The size, polydispersity index (PDI), morphology, and zeta potential of liposomes in milli-Q water were characterised [40]. The particle number of liposomes (particles/ml) was measured by nanoparticle tracking analysis (NTA) using a NanoSight NS300 and the NTA software 3.0 (Malvern Panalytical, UK). Samples were prepared in triplicates, and each sample was measured twice at 25 °C.

### 2.3. Cell culture

The hBMECs within 3 passages were cultured in collagen pre-coated T25 or T75 flasks (Corning® BioCoat™ Collagen 1-coated flask, Life Sciences, USA) containing specialised endothelial cell growth medium (Cell Applications, USA) and maintained in a 5% $CO_2$ humidified atmosphere at 37 °C. The experiments were carried out with cells at passages 4–6.

### 2.4. Determination of cellular uptake of liposomes in hBMECs by confocal microscopy

Confocal laser scanning microscopy (CLSM) was employed to observe the effect of fusogenicity/pH-sensitivity of Rh-PE labelled GSH-PEG-liposomes on their cellular uptake by hBMECs. Cells ($3.5 \times 10^4$ cells in 700 μl of endothelial cell growth media) were seeded in a glass-bottom Eppendorf cell imaging dish (NSW, Australia). After 24 h, the medium was replaced with Rh-PE-labelled GSH-PEG-L or GSH-PEG-pSL in growth media (total lipid concentration of 400 μg/ml) and cultured for 45 min, 4 and 24 h at 37 °C [6]. Cells were then washed with ice-cold PBS (0.01 M, pH 7.4) and fixed for 15 min with 4% paraformaldehyde in 0.01 M PBS at 22 °C. The fixed cells were stained with LysoTracker counter-stained with Hoechst 33342 and mounted with a Prolong™ glass antifade for observation. Images of the cells were acquired using the 63× oil immersion objective of a Zeiss LSM 710 inverted confocal laser microscope equipped with Zeiss Zen advanced imaging software (Carl Zeiss, Germany). Acquired images were analysed using Fiji software, version 1.6 (Bethesda, Maryland, USA), to estimate the mean fluorescence intensity (FI) of Rh-PE (representing the membrane of liposomes) in hBMECs. Individual cells with no bias were manually selected as regions of interest to avoid background interference with the software.

### 2.5. Intracellular trafficking and exocytosis by live-cell imaging

Next, we examined whether the internalised liposomes and their payloads were sorted differently within the hBMECs based on the pH-sensitivity of liposomal components. To achieve this, we investigated the intracellular trafficking of calcein/Rh-PE-labelled GSH-PEG-L or GSH-PEG-pSL in hBMECs pretreated with LysoTrackerTM Deep Red (short for LysoTracker) and a nuclear stain using confocal live-cell imaging aided by colocalisation analysis [38]. Briefly, hBMECs were seeded in Collagen 1 pre-coated Ibidi 8-well chambered slides ($2.5 \times 10^4$ cells/well in 300 μl of endothelial cell growth medium). After 24 h, cells were stained with LysoTracker (100 nM) and Hoechst 33342 for 90 and 20 min, respectively, at 37 °C, then washed. 2–3 cells were chosen in a differential interference contrast (DIC) channel. Then, calcein and Rh-PE dual-labelled liposomes dispersed in a growth medium at 250 μg/ml were added to the cells and maintained at 37 °C and 5% $CO_2$ in the live-cell incubator system. Confocal time-series images were immediately acquired with a Zeiss LSM 710 inverted confocal microscope at regular intervals of 5 min over a 2 h period by bi-directional, sequential scanning to ensure spectral separation of fluorophores. Calcein was excited by a 488 Argon laser (20% intensity), while Rh-PE (Ex/Em 560/583) and LysoTracker (Ex/Em 647/668) were excited by a 633 helium–neon laser (20% intensity).

In the second experiment, to monitor the exocytosis of internalised liposomes without interference by the continued entry of liposomes, hBMECs pre-stained with LysoTracker and Hoechst 44432 were incubated with calcein/Rh-PE-labelled liposomes (in growth medium) for 1 h. Cells were thoroughly washed and cultured in a fresh serum-free medium before confocal time-series imaging over a 2 h period.

For both experiments, images were analysed using Fiji software, version 1.6 (Bethesda, Maryland, USA), to estimate the colocalisation of liposomes (Rh-PE or calcein) with LysoTracker, a dye for tracking of acidic organelles such as endo-lysosomes (endosome and lysosome). Individual cells were manually selected as regions of interest to avoid background interference with the software. A scatter plot was generated from the pixel intensities of channels A (LysoTracker) and B (calcein or Rh-PE), which served as coordinates for a dot on the graph. When a perfect association exists between the two channels, the dot cloud takes the shape of a line and then spreads out in a partial colocalisation. Pearson's correlation coefficients ($r$) were calculated using the colocalisation threshold plugin [39]. In this representation, the $r$ value varies from $-1$ to $+1$, where $-1$ represents inverse correlation (exclusion), zero, the absence of correlation, and $+1$, a complete correlation. Graphs for the correlation coefficients of calcein or Rh-PE and LysoTracker against time were plotted by importing the tabular results from Fiji into GraphPad Prism 7.0.

### 2.6. Exocytosis of liposomes from hBMECs

To further understand the effect of pH-sensitivity on exocytosis of GSH-PEG-liposomes and payload, possible carriers for extruded liposomes from liposome-treated hBMECs into the medium were isolated by the differential centrifugation protocol, which is widely used for the collection of natural EVs. The isolated EVs, mEVs, and sEVs fractions correspond to the increasing centrifugation speed, 10,000 g and 100,000 g, respectively. In addition, natural EVs (typically between 30 nm and 1 μm) [34,41] derived from untreated hBMECs were used as control.

#### 2.6.1. Isolation of extracellular vesicles released from cells

Briefly, hBMECs ($10^7$ cells in collagen 1 pre-coated T 175 flask) were incubated with calcein/Rh-PE labelled GSH-PEG-L or GSH-PEG-pSL for 2 h at 37 °C, before washing and re-incubation in fresh serum-free medium for 24 h at 37 °C, to allow for exocytosis occur. The EV-containing medium was collected and subjected to differential centrifugation, a most commonly used protocol for isolating natural EVs from cells and debris [35,42]. The method involves low-speed centrifugation at 300$g$ for 10 min (to sediment cells), then 2000 $g$ for 20 min (to sediment dead cells, debris, followed by a 10,000 $g$ centrifugation for 30 min to sediment mEVs (150–1000 nm). Finally, the supernatant was ultracentrifuged at 100,000 $g$ for 70 min to sediment the sEVs (20–150 nm). All centrifugation steps were carried out at 4 °C. The mEVs and sEVs pellets were resuspended in PBS for characterisation.

#### 2.6.2. Characterisation of the isolated EVs

The particle number and size of each fraction of the isolated vesicles were analysed using NS300 NanoSight fitted with a NS300 flow-cell top plate and a 405 nm laser [43]. Samples were diluted with PBS at different concentrations (1:100 to 1:10) and analysed at 25 °C with gain adjustments and automatic settings. Each single measurement consisted of three 30-s videos at camera level 10. The detection threshold was set at 4, and data acquisition and processing were performed using the NTA 3.0 software.

Also, the vesicle pellets were lysed using RIPA buffer with sonication for 20 min on ice. After centrifugation at 10,000 $g$, the FI of calcein and Rh-PE in the supernatant was analysed with a BioTek™ Synergy™ 2 Multi-Mode Microplate Reader (BioTek Instruments, Inc, USA) set at Ex/Em wavelength of 495/515 nm for calcein and 560/583 nm for Rh-PE, respectively. Natural EVs from untreated cells were used as background fluorescence.

The morphology and lamellar structure of frozen samples of the isolated vesicles was viewed with Cryo-TEM (Tecnai 12 electron microscope, FEI, Hillsboro, USA) as previously described [44,45]. Furthermore, the isolated vesicles from fluorescent liposome (calcein/Rh-PE)-treated cells were dispersed in PBS and viewed under a fluorescent microscope (Nikon Eclipse E400, Microscope Central, USA).

### 2.7. Confirmation of cellular origin of vesicles by detection of protein marker

To clarify that internalised liposomal contents were repacked and extruded by the hBMECs, the sEVs or mEVs fragments isolated from calcein labelled liposome-treated hBMECs were examined for the presence of endothelial protein marker, CD144, along with CellTracker™ Red CMTPX (referred to as CMTPX) using flow cytometry. The hBMECs prelabelled with CMTPX (0.5 μg/ml for 45 min in serum-free medium at 37 °C) were incubated with calcein-labelled GSH-PEG-L or GSH-PEG-pSL. The cells were washed and re-incubated with a serum-free medium for 24 h to allow for exocytosis. The culture medium was collected and subjected to the standard differential centrifugation protocol (for EV isolation) to isolate the mEVs and sEVs, which was analysed for calcein and CMTPX signal using flow cytometry. In parallel, the isolated vesicles were labelled with an APC-conjugated antibody against CD144. For this, the isolated vesicle pellets were resuspended with an appropriate antibody dilution (0.5 μg/100 μl) in PBS containing 0.15% bovine albumin for 20 min at 4 °C in the dark. The sample was then diluted by 1:5 with PBS and immediately examined with a CyFlow Cube 8 flow cytometer (Sysmex, Germany) [46].

After removing background noise, the gating window for counting mEVs and sEVs was set using forward, and side scatter plots. The isolated vesicles were analysed for calcein (from liposomes) and CMTPX or APC CD144 with the appropriate emission and excitation filters. The Ex/Em wavelengths for calcein were 495/515 nm, while CMTPX and APC CD144 were 577/608 nm and 633/660 nm, respectively. Unstained EVs from non-treated cells were used as control.

### 2.8. Quantitative determination of exocytosed liposomal fluorescent content

The amount of GSH-PEG-liposomes retained or released from hBMECs over time was further estimated based on Rh-PE and calcein fluorescence [47,48]. Briefly, hBMECs suspension ($10^5$ cells in 500 μl of endothelial growth medium) were transferred to Falcon® round-bottom

tubes (STEMCELL Technologies, VIC, Australia) and incubated with calcein/Rh-PE-labelled GSH-PEG-pSL or GSH-PEG-L (400 μg/ml) at 37 °C for 2 h. The cell suspension in different tubes was centrifuged and washed to remove the liposomes outside cells. Cells were then incubated with a fresh medium. At various time intervals (0, 1, 3, 4, 6, or 24 h), the cells were separated from the medium by centrifugation (160 g for 5 min), washed, and lysed with RIPA buffer (20 min in ice, 5 min sonication), followed by ultracentrifugation. The medium (without lysis of any released vesicles) and the supernatant from cell lysis were analysed with a BioTek™ Synergy™ 2 Multi-Mode Microplate Reader (BioTek Instruments, Inc, USA) to estimate the FI of liposomes that were retained or released, respectively. The Ex/Em of calcein and Rh-PE were set at 495/515 nm and 560/583 nm, respectively. At different time points, the FI in cell lysates was compared with zero time-point value (100%).

### 2.9. Evaluation of the exocytosis pathway by immunofluorescence

The involvement of Rab11A in the exocytosis of GSH-PEG-liposomes was investigated by immunofluorescence staining of hBMECs with anti-Rab11A antibody. Rab11A, often found on recycling endosomes and MVB [49], is known to direct the sorting of lipid and protein molecules for exocytosis or recycling depending on the endocytosis pathway [50]. Briefly, hBMECs ($5 \times 10^4$ cells) were seeded in a glass-bottom cell imaging dish (Eppendorf, NSW, Australia). After 24 h, the medium was replaced with Rh-PE-labelled GSH-PEG-L or GSH-PEG-pSL suspension (in medium) and cultured for 2 h at 37 °C. Finally, cells were washed and incubated with a fresh medium for 30 min before immunostaining for Rab11A [51], as detailed in supplementary information. The exocytosis pathway was tracked by the colocalisation of Rh-PE fluorescence signals of internalised liposomes and Alexa Fluor 488 for Rab11A.

### 2.10. Transport efficiency of the liposomes across an in vitro BBB model

An *in vitro* BBB model comprising primary hBMECs in BioCoat™ Transwell inserts (1 μm pore size and 0.33 $cm^2$ effective growth area; BD Biosciences) was developed following the reported method [52]. The model was validated by measuring the apparent permeability of FITC dextran (10 kDa) [53] and the transendothelial electrical resistance (TEER) with an Evom2 Epithelial Voltammeter (World Precision Instruments, Florida USA) before being used to compare the transport of Rh-PE labelled liposomes [54]. Briefly, the lower and upper compartment medium was replaced with 0.6 ml of serum-PBS (0.01 M, pH 7.4 containing 2% v/v FBS). Rh-PE labelled liposomes (400 μg/ml suspended in growth medium) were added to the upper compartment. The whole setup was cultured at 37 °C. At 0.5, 1, 3, 6, 8, and 24 h, the inserts were transferred to new wells with fresh serum-PBS. The fluorescence intensity of Rh-PE in the lower compartments was determined using a microplate reader (Ex/Em:568/583 nm). The TEER of the *in vitro* BBB was re-validated at the end of the study.

### 2.11. Statistical analysis

Statistical analysis was performed by one-way analysis of variance (ANOVA) for multiple groups with Tukey's multiple comparisons test using GraphPad Prism 7.01 (GraphPad Software Inc., CA, USA). A p-value of less than 0.05 was considered statistically significant.

## 3. Results and discussion

### 3.1. Characteristics of GSH-PEG-liposomes

The GSH-PEG-L and GSH-PEG-pSL had similar zeta potential (−31.3 ± 3.7 mV and −30.9 ± 1.0 mV), and particle size (108 ± 2.5 nm or 107.7 ± 8.4 nm) and a narrow size distribution (PDI <0.11 ± 0.01). The liposome concentration (10 mg lipids/ml) was (4.8–5.7) × $10^{13}$ and (6.4–8.0) × $10^{13}$ particles/ml for GSH-PEG-L and GSH-PEG-pSL, respectively, while their cryo-TEM images showed mostly unilamellar with few double-walled structures (Fig. S1).

### 3.2. Cellular uptake of GSH-PEG-liposomes by hBMECs

The mean fluorescence intensity (FI) of Rh-PE (Fig. 1A) from acquired confocal images (Fig. 1B) after incubation of hBMECs with GSH-PEG-liposomes at different time points indicated that the cellular uptake of both liposomes was not significantly different ($p > 0.05$) within 45 min. The GSH-PEG-L nearly attained its maximal cellular uptake at 45 min with a slight increase at 4 h followed by a slight decrease at 24 h. By contrast, the FI of GSH-PEG-pSL treated cells increased over time, significantly higher ($p < 0.05$) at 4 h (1.35-fold) and 24 h (1.6-fold) compared to GSH-PEG-L treated cells. The superior cellular retention was previously attributed to the fusogenic properties of DOPE in GSH-PEG-pSL, which increase the cellular uptake [25].

### 3.3. Intracellular trafficking and exocytosis by live-cell imaging

Live-cell imaging further revealed the internalisation followed by intracellular trafficking of the calcein/Rh-PE-labelled liposomes and exocytosis from the living hBMECs (Fig. 2). The LysoTracker, highly selective for acidic organelles, can be linked to the endo-lysosomes, as the proton pump effect lowers the lumenal pH [55]. GSH-PEG-L-treated cells (Fig. 2A) showed a weak calcein and strong Rh-PE fluorescence signal as early as 5 min, which progressively colocalised in the endo-lysosomes (located around the nuclei) over the 2 h period. By contrast, a strong calcein fluorescence was found in GSH-PEG-pSL-treated cells as early as 30 min adjacent to the endo-lysosomes, which progressively increased over the 2 h period. A weak Rh-PE fluorescence signal was observed as early as 5 min, which gradually increased and more colocalised with the endo-lysosomes over time (Fig. 2B). Following endocytosis of the liposomes, the extrusion of oblong-to-spherical-shaped vesicles of varying sizes (200 nm to occasionally as large as 5 μm) was observed which was

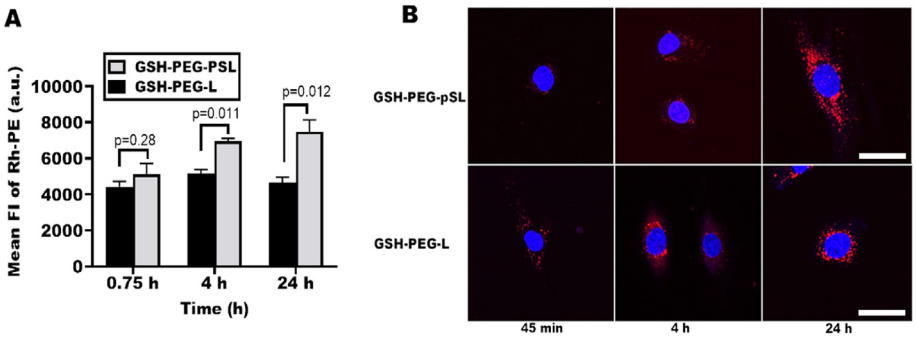


**Fig. 1.** Internalised GSH-PEG-L and GSH-PEG-pSL by hBMECs over time: A) fluorescence intensities of Rh-PE in liposomes (mean ± SD, n = 3 wells), B) Confocal images of hBMECs. Rh-PE fluorescence (red) represents the liposome membrane. The fluorescence signal in blue represents the cell nucleus. The scale bar is 20 μm.

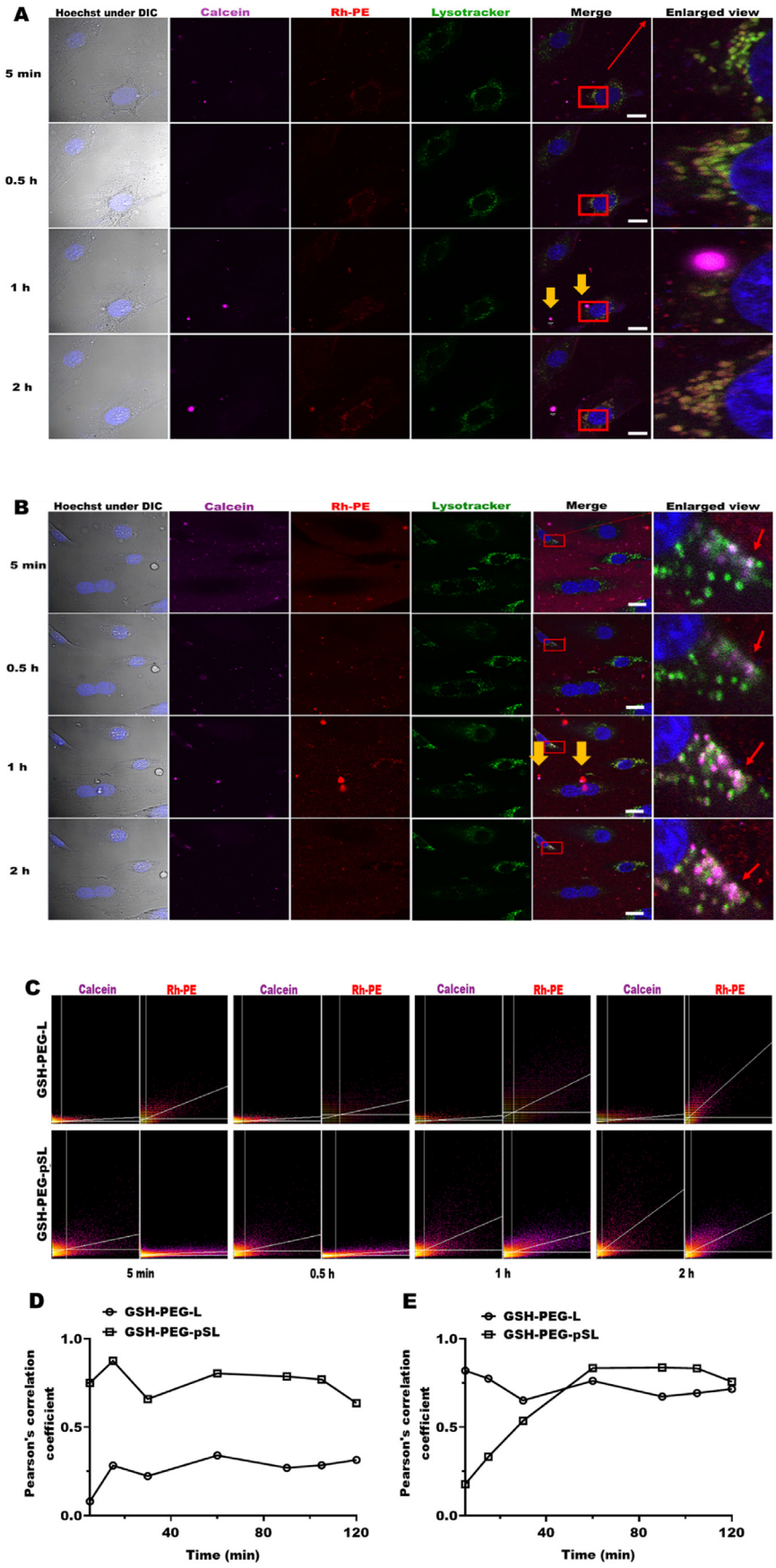


**Fig. 2.** Live-cell CLSM images of hBMECs co-existing with A) GSH-PEG-L and B) GSH-PEG-pSL over 2 h. Uptake of GSH-PEG-L mainly led to the release of vesicles from the cells from approximately 1 h (arrows). C) Scatter plot from calcein- or Rh-PE-LysoTracker channels, show dot cloud along the median line, indicating colocalisation of dual-labelled liposomes with endo-lysosomes. Pearson's correlation coefficients for colocalisation of D) calcein or E) Rh-PE with LysoTracker in hBMECs when co-existing with GSH-PEG-liposomes for 2 h. Calcein (magenta) and Rh-PE (red) represent the liposomal core and membrane, respectively. LysoTracker was used to label the late endo/lysosomal regions (green) and Hoechst 33342 (blue) for nuclei. The scale bars in A) and B) is 20 μm.

sustained over 2 h from GSH-PEG-L-treated cells, while in GSH-PEG-pSL-treated cells, these occurred from around 30 min to 1 h.

Analysis of acquired images as scatter plots of pixel intensities show differing degrees of colocalisation of the two types of liposomes with endo-lysosomes (Fig. 2C). For GSH-PEG-pSL-treated cells, the scatter plots of calcein-LysoTracker channels displayed a spread of the dot cloud away from the median line, indicating decreased colocalisation of GSH-PEG-pSL content with endosomes, while the Rh-PE-LysoTracker channels were aligned. Conversely, in GSH-PEG-L-treated cells, the scatter plot from calcein or Rh-PE and LysoTracker channels with dot clouds aligned to the median line showing the colocalisation of internalised GSH-PEG-L (membrane and content) with endo-lysosomes.

The above findings are consistent with the Pearson's correlation coefficient (r) generated from calcein (Fig. 2D) or Rh-PE (Fig. 2E) with LysoTracker. For GSH-PEG-pSL, relatively stable high $r$ values from calcein-LysoTracker channels were observed (approximately +0.7) over time but dropped at 2 h. Instead, the Rh-PE-LysoTracker had an initial low $r$ value, which increased within 1 h (to approximately +0.8), followed by a slight decrease by 0.1 at 2 h, indicating fusion of GSH-PEG-pSL membrane but endosome escape of calcein. Conversely, for GSH-PEG-L, the $r$ values were low (<+0.3) for the calcein-LysoTracker channels but high in the Rh-PE-LysoTracker channels (>+0.7). This suggests the retention of calcein of GSH-PEG-L within endo-lysosomes.

To further examine intracellular trafficking without cellular uptake interference, we performed live-cell imaging of liposome-pretreated hBMECs. Most endo-lysosomes of GSH-PEG-L-treated cells were filled with GSH-PEG-L, and exocytosis of vesicles containing calcein, Rh-PE, and LysoTracker was observed (Fig. 3A, D and Movie S1). This was accompanied by a gradual loss of both Rh-PE and LysoTracker from the cells, possibly due to the extrusion of EVs of low intra-vesicular pH enclosing GSH-PEG-L.

Supplementary data related to this article can be found at https://doi.org/10.1016/j.mtbio.2022.100212.

Conversely, the GSH-PEG-pSL-treated cells revealed the presence of strong and disseminated calcein fluorescence signals in the cytoplasm, with some endo-lysosomes still colocalizing with liposomes, followed by the extrusion of vesicles containing only Rh-PE and LysoTracker (Fig. 3B and Movie S2).

Supplementary data related to this article can be found at https://doi.org/10.1016/j.mtbio.2022.100212.

Declining $r$ values (Rh-PE vs LysoTracker channels, Fig. 3C) were observed in both liposomes. However, it may suggest different cellular events such as exocytosis of GSH-PEG-L evidenced by the gradual depletion of LysoTracker. However, internalised GSH-PEG-pSL fuse with the endosome membrane leading to the release of its content into the cytoplasm and reduced exocytosis of intact liposomes. By comparison, GSH-PEG-L appeared to stay with the endosomes and, thus, retains most of its payload before being extruded from hBMECs, thus completing the transcellular transport process, possibly intact.

These large vesicles (5 μm) are comparable to autophagic bodies (autophagosomes, amphisomes or autolysosomes, lumen pH 5–6) [56,57] of the autophagy pathway based on their low pH and size (2–5 μm) [49]. Amphisomes or autolysosomes are formed via the interaction between the autophagosome and late endosome/MVB or lysosomes (containing liposomes) in cells [58,59]. Further studies are required to understand the nature of these large vesicles.

### 3.4. Exocytosis of liposomes from hBMECs

#### 3.4.1. Exocytosis of liposomes and pH-sensitivity effect

Herein, each hBMEC without liposome treatment (control) secreted 417 ± 59 sEVs and 63 ± 29 mEVs in 24 h, similar to the reported EV secretion numbers from endothelial cells [34,60,61].

As shown in Fig. 4A, GSH-PEG-L-treated cells produced 2.6-fold ($p < 0.05$) and 7.9-fold ($p < 0.01$) more sEVs, as well as 4.6-fold ($p < 0.01$) and 2.3-fold more mEVs, than GSH-PEG-pSL-treated cells and control cells, respectively. Conversely, GSH-pSL-treated cells produced significantly 2.9-fold more sEVs ($p < 0.01$) but 2-fold less mEVs than the control cells. The stimulation effect of GSH-PEG-L corresponds with a previous study that demonstrated the FC5 antibody to cause a 4-fold increase in EV production by immortalised human brain microvascular endothelial cells (HCMEC/D3) via the stimulation of receptor-mediated transport [34]. Most recently, doxorubicin-loaded porous silicon nanoparticles (PSiNPs) were also reported to stimulate the production of exosomes almost 34-fold, with a subsequent yield of exosome-sheathed PSiNPs from the cancer cells [62].

Furthermore, we examined the FI of Rh-PE and calcein in the lysates of mEVs and sEVs, representing the liposomal payload and membrane, respectively, in this study. Fig. 4B&C illustrates that the FIs of calcein and Rh-PE in the mEV lysates from GSH-PEG-L-treated cells were 2.5 or 2.7-fold higher than those from GSH-PEG-pSL-treated cells ($p < 0.01$), indicating more exocytosis of GSH-PEG-L than GSH-PEG-pSL through mEV secretion. By contrast, only GSH-PEG-pSL treatment resulted in significant FIs of Rh-PE in the sEV lysates, 2-fold of the natural sEV lysates ($p < 0.05$). However, both liposome treatments produced calcein FIs (GSH-PEG-pSL-treated being slightly lower), approximately 4-fold stronger ($p > 0.05$) than that of the natural sEV lysates. This suggests both liposomes' payloads were packed in the sEVs before being extruded from the cells, while only the GSH-PEG-pSL membrane was found in the sEVs, which may be the sEV membrane. This is linked to the fusion of GSH-PEG-pSL bilayers containing Rh-PE with the endosomal membrane, one of the proposed mechanisms for 'endosome escape' of pSL [39]. The other two mechanisms are the collapse of pSL in the low pH of the endosomal lumen leading to the diffusion of the content to cytosol and rupture of endosomes [63]. Calcein can only be released into the cytosol through these two pathways because of its hydrophilic nature.

Size analysis of the collected vesicles revealed that the mEVs produced by GSH-PEG-L-treated cells were 20 nm smaller and scientifically more negatively charged (by 19 mV) than those of the natural mEVs secreted from hBMECs (control) (Fig. 4D). The charge was close to those of the liposomes (−30 mV). On the other hand, both the sEVs and mEVs secreted from GSH-PEG-pSL-treated cells were negatively charged and smaller than the natural sEVs and mEVs. It would be interesting to carefully isolate and evaluated the large vesicles (5 μm in size) in the future as they are presumably lost with cell debris during the centrifugation process in this study.

It is also worth noting that liposome enclosure in some sEVs or mEVs could increase their density and sedimentation into a different isolated EV fraction than natural EVs during separation by differential centrifugation method. According to Stokes' law, the settling velocity of solid particles in a liquid is maximised by a significant density difference (among other factors) between solids and liquid [33]. This is evidenced by the reduced size of mEV fractions from liposome-treated cells compared to natural mEVs (Fig. 4D). Therefore, the term mEVs for liposome-treated cells could signify a mix of natural mEVs secreted by hBMECs along with mEVs and sEVs enclosing liposomes.

The cryo-TEM images revealed an oblong-to-spherical-shaped morphology of the vesicles from liposome-treated and control dissimilar to the internalised GSH-PEG-liposomes (Fig. 4D). Interestingly, the sEVs and mEVs extruded by GSH-PEG-L-treated cells appear to enclose single or groups of spherical structures resembling GSH-PEG-L, which was dissimilar to the sEVs from GSH-PEG-pSL-treated cells, and spherical like the EVs from control cells. The mEVs secreted from GSH-PEG-pSL-treated cells had a darker outer surface layer. This was not present in similar vesicles produced by GSH-PEG-L-treated cells or control vesicles, signifying the interaction of GSH-PEG-pSL with the plasma membrane of

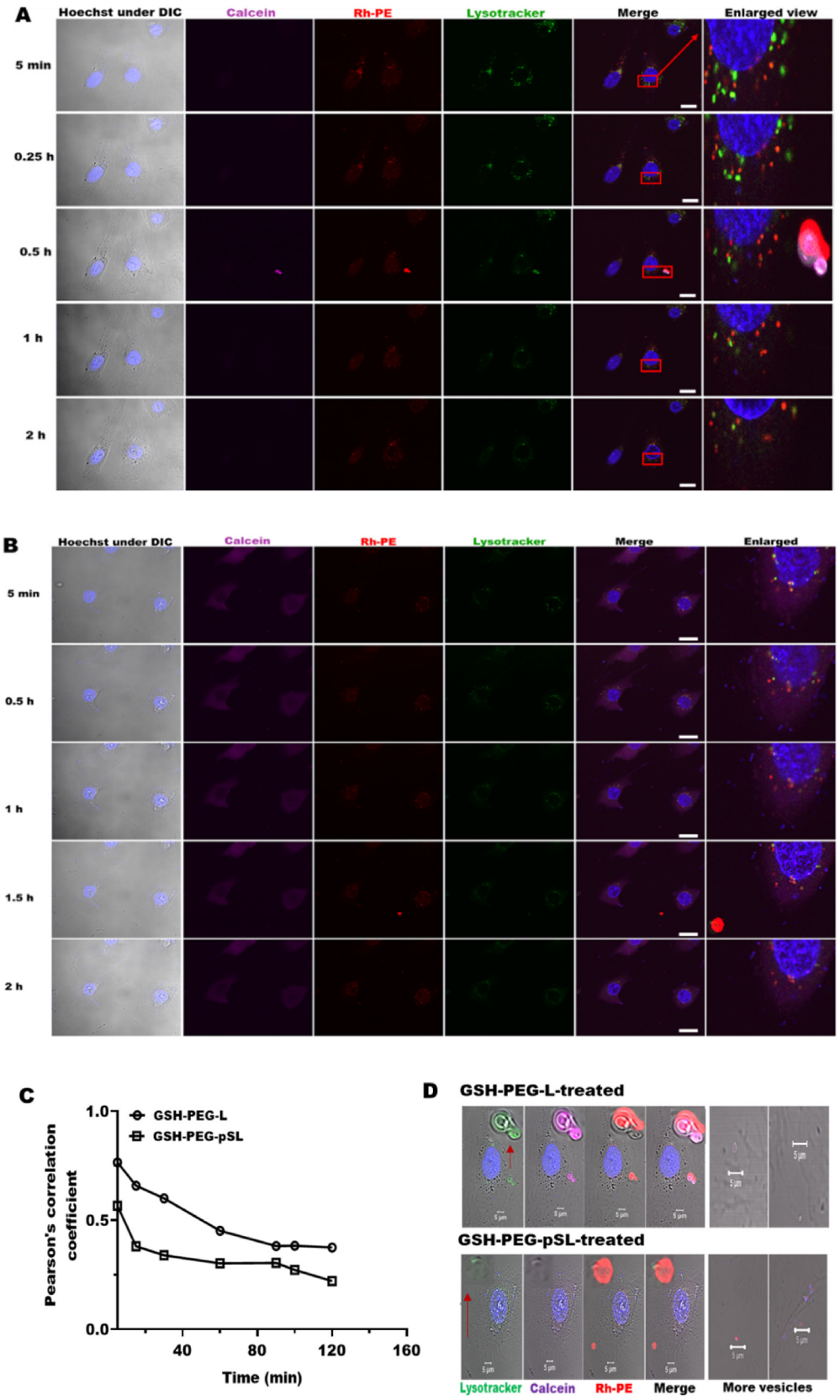


**Fig. 3.** Live-cell CLSM images of hBMECs pretreated with calcein/Rh-PE dual-labelled liposomes for 1 h and before washing and re-incubation in fresh medium: Cells pretreated with A) GSH-PEG-L, or B) GSH-PEG-pSL. C) Pearson's correlation coefficients for colocalisation of Rh-PE (liposomes membrane) with LysoTracker (green) of hBMECs. Calcein (magenta) and Rh-PE (red) represent the liposome's core and membrane, respectively. LysoTracker indicates late endo/lysosomal regions. Hoechst 33342 (blue) was used as a nuclear stain. D) Images of vesicles secreted from GSH-PEG-L pretreated cells enclosing calcein, Rh-PE, and LysoTracker, but no calcein signal was observed in those GSH-PEG-pSL pretreated cells. Scale bars are 20 μm in A and B, and 5 μm in D.

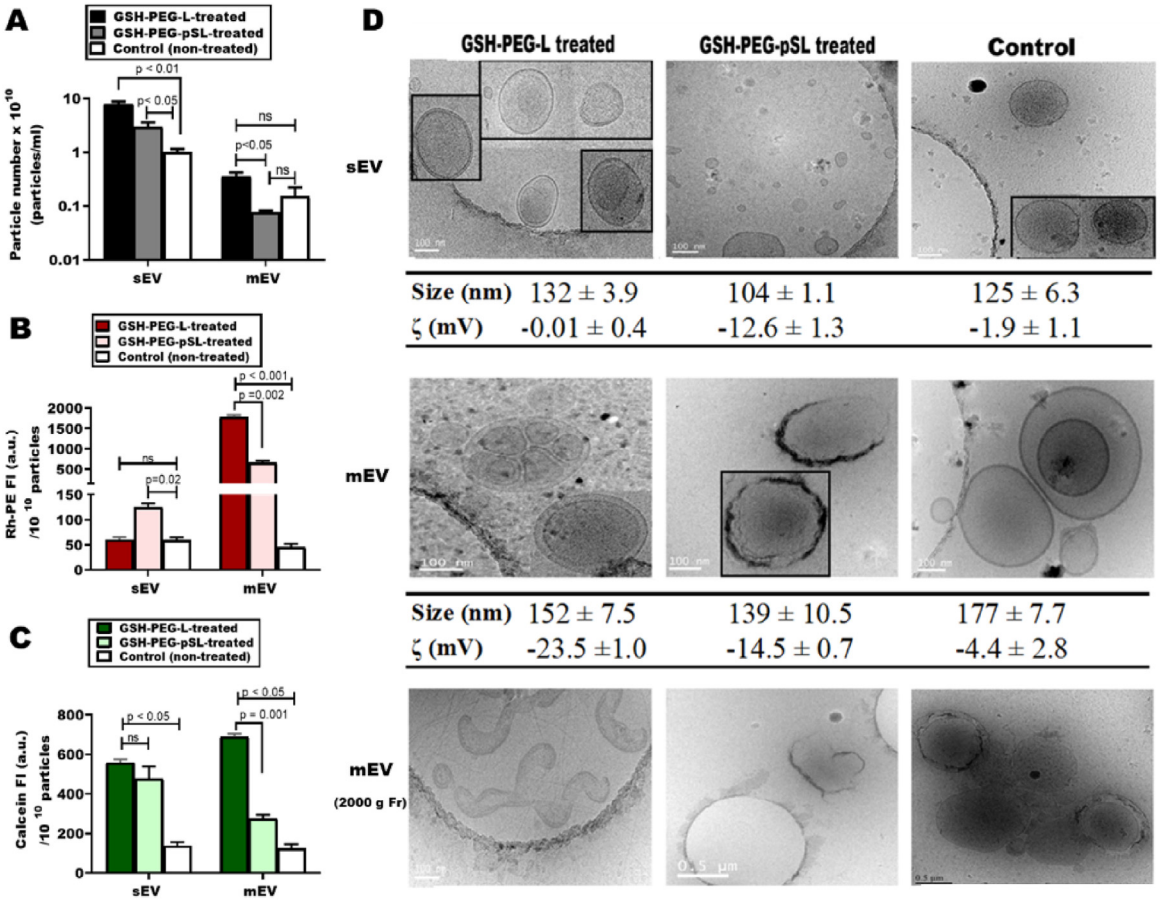


**Fig. 4.** Physicochemical properties of isolated vesicles from hBMECs following treatment with GSH-PEG-L and GSH-PEG-pSL for 2 h versus EVs from non-treated cells (control). A) the particle numbers in the sEV and mEV fractions; B & C) the FIs of Rh-PE (B) and calcein (C) in the EV lysates; D) Vesicle size, zeta potential and morphology under cryo-TEM. Vesicles secreted from cells were fractioned at various centrifugation speeds of 2000 g– defined as mEV 2000 g fraction, 10000 g – mEVs and 100,000 g – sEVs.

hBMECs. Furthermore, mEV-2000 g Fr, especially from GSH-PEG-L treated cells, were sac-like structures different from the natural EVs of control cells obtained at 2000 g centrifugation speed. The observed structures could be vesicles that ruptured during sample preparation due to less rigid membrane or isolated in that form. The morphology of the vesicles, especially for the control EVs, was similar to recent reports on cryo-electron microscopy of EVs from cerebrospinal fluid and other human biofluids or cell-culture conditioned medium [44]. Taken together, these findings depict more exocytosis of GSH-PEG-L as whole liposomes than GSH-PEG-pSL and the presence of the former in large-sized vesicles.

### *3.4.2. Confirmation of cellular origin of vesicles by detection of protein marker*

The sEVs from GSH-PEG-L-treated cells were positive for the CMTPX signal and contained calcein (Fig. 5A), suggesting their origin from hBMECs. Surprisingly, sEVs from GSH-PEG-pSL-treated cells had calcein but without CMTPX signal due to possible destruction of the latter during intracellular processing of GSH-PEG-pSL. On the other hand, the mEVs (fraction) from GSH-PEG-L and GSH-PEG-pSL-treated cells were positive for calcein and CMTPX (Fig. 5B). This indicated the cells used mEV to export intact internalised liposomes and their content, including those in the cytoplasm, via outward budding of the plasma membrane.

Furthermore, the mEVs and sEVs extruded from GSH-PEG-L or GSH-PEG-pSL-treated cells (Fig. 5C and D) were positive CD144. CD144 is a cell marker that is also enriched on endothelial cell-derived EVs [64]. The above data provided strong evidence that the isolated vesicles were extruded from the hBMECs, possibly comprising a mixture of natural EV and liposome-EV hybrids but were not simply modified liposomes. Notably, the CD144 antibody-negative and CMPTX-negative staining control EVs had no CMTPX or CD144 signal, confirming that internalised liposomal contents (calcein) were repacked into CD144 + ve and CMTPX + ve vesicles, particularly mEVs. This finding is in line with a recent report which demonstrated that endocytosed lipid nanoparticle-messenger RNA (LNP-mRNA) were re-packaged into EVs and were then extruded from the cells [65]. However, they did not quantify the EV number.

### *3.4.3. Quantitative determination of exocytosed liposomes*

The luminal exocytosis from liposome-treated hBMECs (in the absence of liposome contents) in media was assessed over 24 h. The quantified calcein FI released in the surrounding medium of GSH-PEG-L-treated hBMECs was about 2-fold more than GSH-PEG-pSL-treated hBMECs and attained a maximum during the first 6 h (Fig. 6A). In comparison, the FI of Rh-PE released into the media increased over 24 h with little difference between liposomes (16.5 ± 1.9% vs. 17.3 ± 0.5% of the total FI in cells at time zero) (Fig. 6B). A corresponding reduction of Rh-PE FI retained in the cells over time, as measured in the cell lysates, was found in GSH-PEG-L-treated cells and GSH-PEG-pSL-treated cells (Fig. 6C). However, a 21% increase in retained GSH-PEG-pSL and not

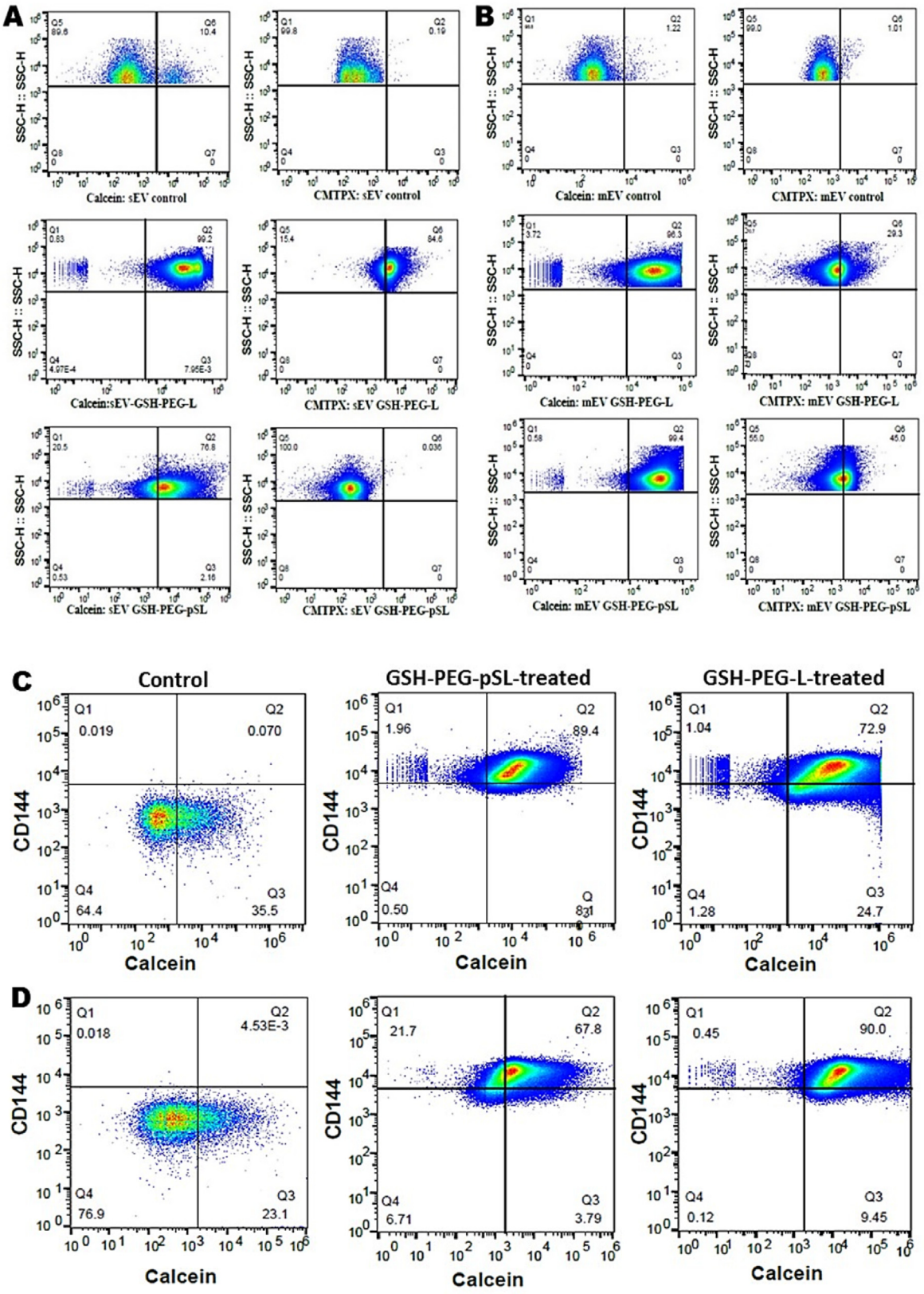


**Fig. 5.** Isolated sEVs (A) and mEVs (B) extruded from liposome-treated hBMECs versus natural sEVs and mEVs showing side-scatter versus forward scatter or calcein/CMTPX dot plot; CD144 protein versus calcein (liposomal content) dot plot for mEVs (C) and sEVs (D) compared with the naturally secreted sEVs and mEVs (controls).

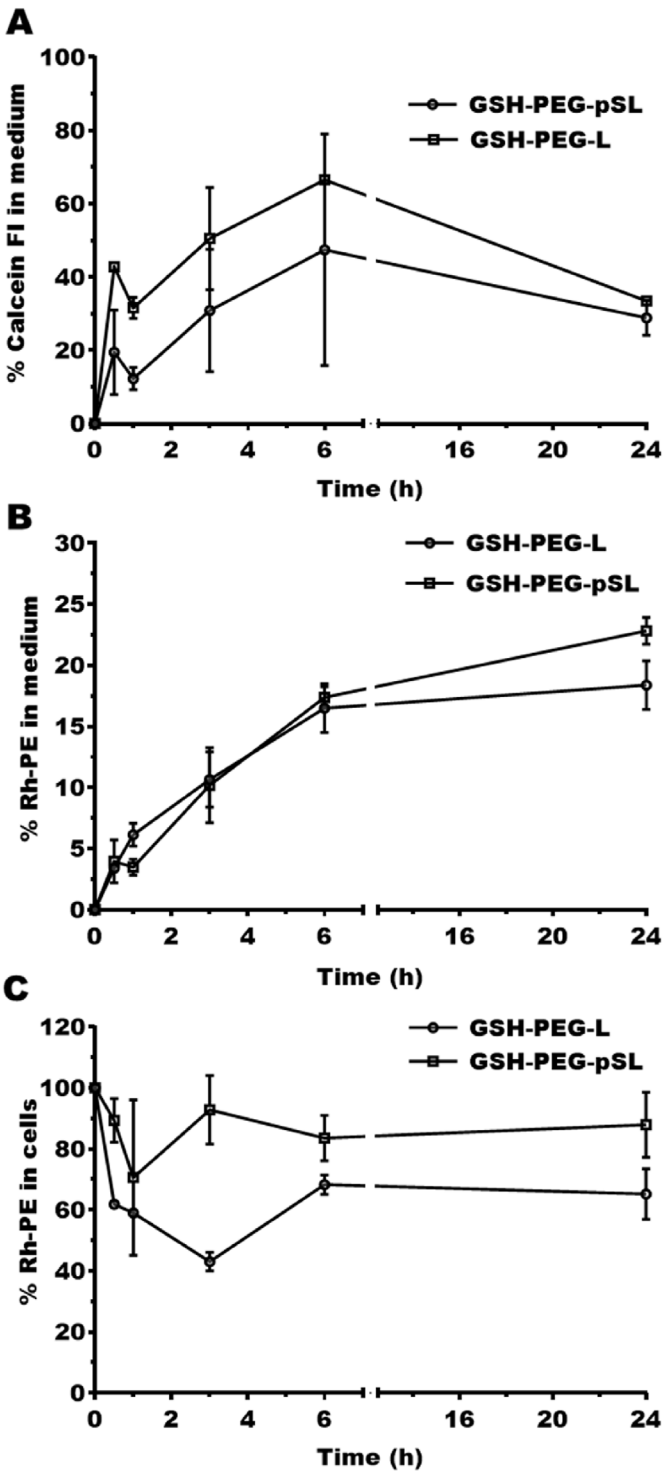


**Fig. 6.** Quantitative determination of exocytosed liposomal fluorescent content of A) calcein (the liposomes content) released in the medium, and Rh-PE (liposomes membrane) B) released in the medium or C) retained in a cell lysate following incubation with fresh medium at 37 °C for 24 h. The Rh-PE and calcein FI in cell lysates immediately after 2 h incubation with liposomes (defined as time 0) were set 100%. Data are means ± SD, n = 3.

GSH-PEG-L of cell lysates from 1 to 3 h could be attributed to re-entering of exocytosed GSH-PEG-pSL due to their fusogenic nature. Similarly, this higher retention of internalised GSH-PEG-pSL in analysed hBMECs lysates is consistent with the confocal microscopy evaluation findings of cellular uptake or retention (Fig. 1).

The total Rh-PE FIs retained and released from GSH-PEG-pSL-treated cells at 6 h and 24 h were close to 100%. In contrast, the corresponding values were only 88% and 80.4% in GSH-PEG-L-treated cells, which may be due to lysosomal degradation or endosome entrapment.

### 3.5. Evaluation of the exocytosis pathway by immunofluorescence

Additionally, confocal images showed that Rab11A regulated the exocytosis of GSH-PEG-liposomes in hBMECs after 2 h of liposome treatment (Fig. S2) for images of individual channels). The fluorescence signal of Rab11A was colocalised with the Rh-PE labelled GSH-PEG-L both at the perinuclear region (red arrows) and close to the plasma membrane along the actin filaments. The Rh-PE fluorescence of GSH-PEG-pSL also colocalised with Rab11A, but mainly at the perinuclear region.

In the cells, more GSH-PEG-L colocalised with Rab11A towards the plasma membrane than in the endo-lysosomes, while GSH-PEG-pSL colocalised with Rab11A at the perinuclear area, especially in endo-lysosomes (Fig. S2). These findings correspond with recent reports, showing Rab11A is transported to the cell periphery with recycling vesicles, directly regulating vesicle exocytosis at the plasma membrane [50]. Thus, this study may suggest that Rab11A regulation of more GSH-PEG-L trafficking towards the plasma membrane of hBMECs relates to the extrusion of more GSH-PEG-L via EVs. Moreover, Rab11A is involved in autophagosome–endosome fusion to form an intermediate organelle, amphisomes [66], further suggesting that the large acidic vesicles released from liposome-treated hBMECs are most likely to be amphisomes/autophagosomes.

### 3.6. Transcellular efficiency of liposomes across the in vitro BBB model

The hBMECs monolayer model cultured for 7 days displayed a $P_{app}$ ($2.8 \pm 0.1$) x $10^{-6}$ $cm^2/s$ to FITC dextran (10 kDa) TEER ($120.52 \pm 13.5$ $\Omega$ $cm^2$) values, comparable to the previously reported value [52], with no significant change following further culture at day 10 (Fig. 7A &B), suggesting the successful establishment of the BBB model. The transcellular transport efficiency measured with Rh-PE FI over 24 h of GSH-PEG-L was 2.5-fold higher than GSH-PEG-pSL ($p < 0.001$) (Fig. 7C). Rh-PE has two long lipophilic tails (C14) thus has strong affinities with biomembranes. Therefore, the only pathway to cross the *in vitro* BBB model was via the transcellular pathway, namely, secretion of liposome-EV hybrids. In contrast, GSH-PEG-pSL underwent endosome escape via liposome-endosome fusion [19,20], and therefore reduced exocytosis of the liposomes. It is worth noting that lipophilic small molecules loaded in the pSL may still exploit the passive diffusion from the cytoplasm and cross the BBB.

Overall, the present study revealed a phenomenon of how liposomes underwent transcytosis through hBMECs using cell line and monolayer models, either as a natural EV secretion or cellular elimination machinery for 'foreign' nanoparticles. There is a critical need to understand the physiological relevance of these findings in the complex *in vivo* situation. Our BBB model shows that the EVs are extruded from the basolateral (facing the brain) side of the endothelial cells. A question that remains is whether the EVs are equally released to the apical/lumenal side (facing the blood), or polarised. The apical-basal membranes hBMECs differ in their lipid and (glyco-)protein composition with asymmetry expression glucose transporter (influx to brain) [67] and drug efflux transporters [68], possibly to maintain the homeostasis. In addition, understanding the impact of formulation and drug properties on transport to the brain for the wider nanoscale drug delivery systems (such as polymeric or inorganic systems) through post-analysis of brain capillaries for the latter and EV would be of great interest in future research, to correlate the *in vitro* data.

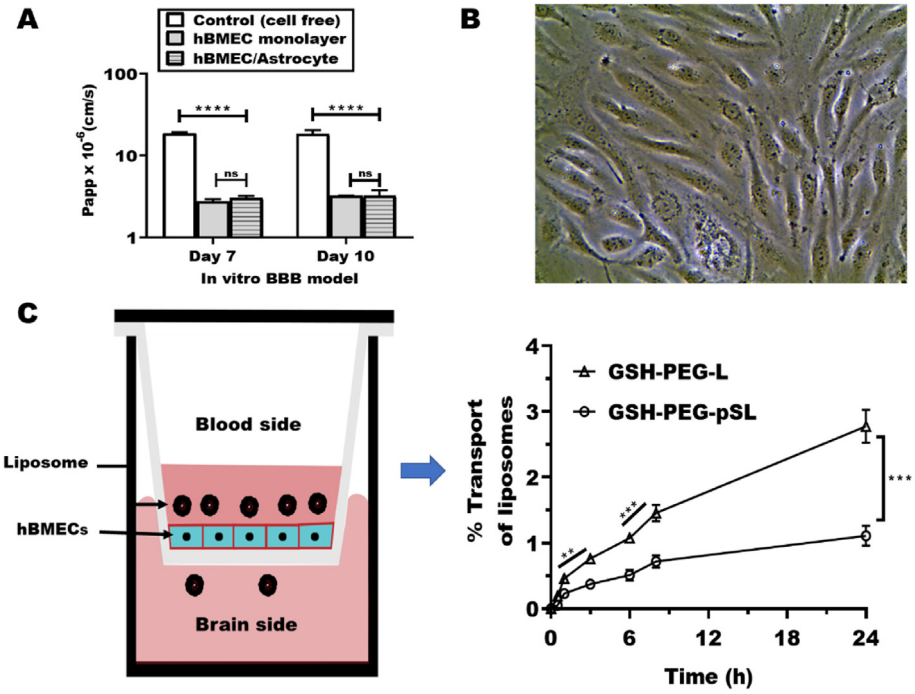


**Fig. 7.** Investigating transport of liposomes across an *in vitro* BBB model: a) $P_{app}$ of FITC dextran (10 kDa) across the *in vitro* BBB models at day 7–10; b) light microscopic images of hBMECs monolayer forming a tight barrier at day 7 post-seeding with a cobble-stone appearance; and c) the transport efficiency of Rh-PE labelled GSH-PEG-L versus GSH-PEG-pSL across the *in vitro* BBB monolayer model, measured as the fluorescence of Rh-PE in the brain side compartment (Rh-PE is unable to cross the BBB by diffusion as a highly lipophilic molecule unless via alternative transport pathway.

## 4. Conclusions

To understand the transport mechanisms of liposomes across brain endothelial cells, herein, the cellular trafficking of liposomes was revealed, with a focus on exocytosis using hBMEC models. After endocytosis, GSH-PEG-L and GSH-PEG-pSL followed the endolysosomal pathway. GSH-PEG-L were extruded from the cells as whole liposomes, sheathed individually or as a group in a membrane, promoting the release of mEVs and sEVs of hBMECs. Furthermore, most of the mEVs and sEVs produced by liposome-treated cells were confirmed to be of endothelial origin evidenced by the CD144 marker. By contrast, due to the pH-sensitivity, GSH-PEG-pSL underwent 'endosome escape', and subsequent reduction in the exocytosis of these liposomes. This pH-sensitivity-mediated cytoplasmic release which may limit the transport efficiency across the BBB to the brain if the drugs (such as proteins) can hardly diffuse through the endothelial cells. Taken together, this study demonstrated that liposomes might utilize EV secretion to achieve transcytosis while the pH-sensitivity increased cytosolic delivery but suppresses transcellular transport efficiency via the exocytosis pathway.

## Author contributions

ZW conceived the study. ZW, JR and LC contributed to the study design. JR performed all the experiments with some assistance from SP and MT; ZW, JR, LC, and DS interpreted the data; JR, with the supervision of ZW, drafted the manuscript, and all other authors reviewed and revised the manuscript.

## Statement of significance

Liposomes have been extensively researched as nanocarriers to improve drug delivery to the brain owing to their potentials to cross the blood brain barrier (BBB). Unveiling the transport mechanisms of liposomes across the brain endothelial cells, the primary functional component of BBB, could offer new insight to researchers on optimal liposomal formulation design. Herein we utilised a human brain endothelial cell line and an endothelial cell monolayer BBB model to demonstrated that liposomes could be exocytosed as whole liposomes via secretion of extracellular vesicles (EV). We used various techniques to capture the dynamic processes of transcytosis of liposomes and demonstrated the impact of liposomal pH-sensitivity on this process as well as the cellular responses upon interaction with these nanoparticles. The methodology we employed may be used for machinery research of nanoparticles to cross other biological carriers lined by endothelial cells. Additionally, the secreted EV-liposome hybrids from cells may serve as novel nanobiomaterials.

## Declaration of competing interest

The authors declare that they have no known competing financial interests or personal relationships that could have appeared to influence the work reported in this paper.

## Acknowledgment

The authors acknowledge the financial support from Auckland Medical Research Foundation (Grant number: 1118019), and JR's doctoral scholarship from Schlumberger Foundation Faculty for the Future. We would also like to thank Jacqui Ross for her technical support for the live-cell imaging experiments.

## Appendix A. Supplementary data

Supplementary data to this article can be found online at https://doi.org/10.1016/j.mtbio.2022.100212.

## References

[1] H.F. Salem, S.M. Ahmed, A.E. Hassaballah, M.M. Omar, Targeting brain cells with glutathione-modulated nanoliposomes: in vitro and in vivo study, Drug Des. Dev. Ther. 9 (2015) 3705–3727.
[2] P.J. Gaillard, C.C.M. Appeldoorn, R. Dorland, J. van Kregten, F. Manca, J.D. Vugts, Windhorst, G.A.M.S. van Dongen, E.H. de Vries, D. Maussang, O. van Tellingen Pharmacokinetics, Brain delivery, and efficacy in brain tumor-bearing mice of glutathione pegylated liposomal doxorubicin (2B3-101), PLoS One 9 (2014), e82331.
[3] P.J. Gaillard, C.C.M. Appeldoorn, J. Rip, R. Dorland, G. van Dp, Kooij, E.H. de Vries, A. Reijerkerk, Enhanced brain delivery of liposomal methylprednisolone improved

therapeutic efficacy in a model of neuroinflammation, J. Contr. Release 164 (2012) 364–369.
[4] D. Maussang, J. Rip, J. van Kregten, A. van den Heuvel, S. van der Pol, B. van der Boom, A. Reijerkerk, L. Chen, M. de Boer, P. Gaillard, Glutathione conjugation dose-dependently increases brain-specific liposomal drug delivery in vitro and in vivo, Drug Discov. Today Technol. 20 (2016) 59–69.
[5] A. Lindqvist, J. Rip, J. van Kregten, P.J. Gaillard, M. Hammarlund-Udenaes, In vivo functional evaluation of increased brain delivery of the opioid peptide DAMGO by glutathione-PEGylated liposomes, Pharm. Res. (N. Y.) 33 (2016) 177–185.
[6] Y. Hu, J. Rip, P.J. Gaillard, C.M. de Lange Elizabeth, M. Hammarlund-Udenaes, The impact of liposomal formulations on the release and brain delivery of methotrexate: an in vivo microdialysis study, J. Pharm. Sci. 106 (2017) 2606–2613.
[7] W. Zhan, Delivery of liposome-encapsulated temozolomide to brain tumour: understanding the drug transport for optimisation, Int. J. Pharm. 557 (2019) 280–292.
[8] S. Joshi, J.R. Cooke, D.K. Chan, J.A. Ellis, S.S. Hossain, R.P. Singh-Moon, M. Wang, I.J. Bigio, J.N. Bruce, R.M. Straubinger, Liposome size and charge optimization for intraarterial delivery to gliomas, Drug Deliv. Transl. Res. 6 (2016) 225–233.
[9] Y. Chen, J. Sun, Y. Lu, C. Tao, J. Huang, H. Zhang, Y. Yu, H. Zou, J. Gao, Y. Zhong, Complexes containing cationic and anionic pH-sensitive liposomes: comparative study of factors influencing plasmid DNA gene delivery to tumors, Int. J. Nanomed. 8 (2013) 1573–1593.
[10] J. Connor, L. Huang, pH-sensitive immunoliposomes as an efficient and target-specific carrier for antitumor drugs, Cancer Res. 46 (1986) 3431.
[11] Cd Santos Giuberti, R. de Oliveira, C. Eduardo, T.G. Ribeiro Rocha, E.A. Leite, R.G. Lacerda, G.A. Ramaldes, M.C. de Oliveira, Study of the pilot production process of long-circulating and pH-sensitive liposomes containing cisplatin. J, Liposome Res. 21 (2011) 60–69.
[12] A.L.B. de Barros, Ld G. Mota, D.C.F. Soares, M.M.A. Coelho, M.C. Oliveira, V.N. Cardoso, Tumor bombesin analog loaded long-circulating and pH-sensitive liposomes as tool for tumor identification, Bioorg. Med. Chem. Lett 21 (2011) 7373–7375.
[13] M. Chang, S. Lu, F. Zhang, T. Zuo, Y. Guan, T. Wei, W. Shao, G. Lin, RGD-modified pH-sensitive liposomes for docetaxel tumor targeting, Colloids Surf. B Biointerfaces 129 (2015) 175–182.
[14] Y. Zhao, W. Ren, T. Zhong, S. Zhang, D. Huang, Y. Guo, et al., Tumor-specific pH-responsive peptide-modified pH-sensitive liposomes containing doxorubicin for enhancing glioma targeting and anti-tumor activity, J. Contr. Release 222 (2016) 56–66.
[15] T.G. Rocha, S.C. Lopes, G.D. Cassali, E. Ferreira, E.S. Veloso, E.A. Leite, C.F. Braga, L.A.M. Ferreira, D. Balvay, A. Garofalakis, M.C. Oliveria, B. Tavitan, Evaluation of antitumor activity of long-circulating and pH-sensitive liposomes containing ursolic acid in animal models of breast tumor and gliosarcoma, Integr. Cancer Ther. 15 (2016) 512–524.
[16] A. Cerletti, J. Drewe, G. Fricker, A.N. Eberle, J. Huwyler, Endocytosis and transcytosis of an immunoliposome-based brain drug delivery system, J. Drug Target. 8 (2000) 435–446.
[17] Y. Fan, C. Chen, Y. Huang, F. Zhang, G. Lin, Study of the pH-sensitive mechanism of tumor-targeting liposomes, Colloids Surf. B Biointerfaces 151 (2017) 19–25.
[18] Z. Vanić, S. Barnert, R. Süss, R. Schubert, Fusogenic activity of PEGylated pH-sensitive liposomes, J. Liposome Res. 22 (2012) 148–157.
[19] M.M. Yang, W.R. Wilson, Z. Wu, pH-sensitive PEGylated liposomes for delivery of an acidic dinitrobenzamide mustard prodrug: pathways of internalization, cellular trafficking and cytotoxicity to cancer cells, Int. J. Pharm. 516 (2017) 323–333.
[20] M. Kanamala, B. Palmer, H. Ghandehari, W. Wilson, Z. Wu, PEG-Benzaldehyde-Hydrazone-Lipid based PEG-sheddable pH-sensitive liposomes: abilities for endosomal escape and long circulation, Pharm. Res. (N. Y.) 35 (2018) 1–13.
[21] M. Tang, D. Svirskis, E. Leung, M. Kanamala, H. Wang, Z. Wu, Can intracellular drug delivery using hyaluronic acid functionalised pH-sensitive liposomes overcome gemcitabine resistance in pancreatic cancer? J. Contr. Release 305 (2019) 89–100.
[22] V.A. Slepushkin, S. Simões, P. Dazin, M.S. Newman, L.S. Guo, C.M. Pedroso de Lima, N. Düzgüneş, Sterically stabilized pH-sensitive liposomes. Intracellular delivery of aqueous contents and prolonged circulation in vivo, J. Biol. Chem. 272 (1997) 2382–2388.
[23] S. Ferreira Ddos, S.C. Lopes, M.S. Franco, M.C. Oliveira, pH-sensitive liposomes for drug delivery in cancer treatment, Ther. Deliv. 4 (2013) 1099–1123.
[24] R. Villaseñor, J. Lampe, M. Schwaninger, L. Collin, Intracellular transport and regulation of transcytosis across the blood–brain barrier, Cell. Mol. Life Sci. 76 (2019) 1081–1092.
[25] G. Sharma, A.R. Sharma, S.S. Lee, M. Bhattacharya, J.S. Nam, C. Chakraborty, Advances in nanocarriers enabled brain targeted drug delivery across blood brain barrier, Int. J. Pharm. 559 (2019) 360–372.
[26] S. Ayloo, C. Gu, Transcytosis at the blood–brain barrier, Curr. Opin. Neurobiol. 57 (2019) 32–38.
[27] V.M. Pulgar, Transcytosis to cross the blood brain barrier, new advancements and challenges, Front. Neurosci. 12 (2019) 1019.
[28] M. Tamaru, H. Akita, K. Kajimoto, Y. Sato, H. Hatakeyama, H. Harashima, An apolipoprotein E modified liposomal nanoparticle: ligand dependent efficiency as sirna delivery carrier for mouse-derived brain endothelial cells, Int. J. Pharm. 465 (2014) 77–82.
[29] C.J. Wen, L.W. Zhang, S.A. Al-Suwayeh, T.C. Yen, J.Y. Fang, Theranostic liposomes loaded with quantum dots and apomorphine for brain targeting and bioimaging, Int. J. Nanomed. 7 (2012) 1599–1611.
[30] S. Rayamajhi, J. Marchitto, T.D.T. Nguyen, R. Marasini, C. Celia, S. Aryal, pH-responsive cationic liposome for endosomal escape mediated drug delivery, Colloids Surf. B Biointerfaces 188 (2020) 110804.
[31] S. Sindhwani, A.M. Syed, J. Ngai, B.R. Kingston, L. Maiorino, J. Rothschild, P. MacMillan, Y. Zhang, N.U. Rajesh, T. Hoang, J.L.Y. Wu, S. Wilhelm, A. Zilman, S. Gadde, A. Sulaiman, B. Ouyang, Z. Lin, L. Wang, M. Egeblad, W.C.W. Chan, The entry of nanoparticles into solid tumours, Nat. Mater. 19 (2020) 566–575.
[32] E. Silva, L. Barreiros, M.A. Segundo, S.A. Costa Lima, S. Reis, Cellular interactions of a lipid-based nanocarrier model with human keratinocytes: unravelling transport mechanisms, Acta Biomater. 53 (2017) 439–449.
[33] J. Reinholz, C. Diesler, S. Schöttler, M. Kokkinopoulou, S. Ritz, K. Landfester, Volker mailander. Protein machineries defining pathways of nanocarrier exocytosis and transcytosis, Acta Biomater. 71 (2018) 432–444.
[34] I.E. András, M. Toborek, Extracellular vesicles of the blood-brain barrier, *Tissue Barriers* 4 (2016), e1131804.
[35] T. Geng, P. Pan, E. Leung, Q. Chen, L. Chamley, Z. Wu, Recent advancement and technical challenges in developing small extracellular vesicles for cancer drug delivery, Pharm. Res. (N. Y.) 38 (2021) 179–197.
[36] A.S. Haqqani, C.E. Delaney, T.L. Tremblay, C. Sodja, J.K. Sandhu, D.B. Stanimirovic, Method for isolation and molecular characterisation of extracellular microvesicles released from brain endothelial cells, Fluids Barriers CNS 10 (2013), 4-4.
[37] J. Saint-Pol, F. Gosselet, S. Duban-Deweer, G. Pottiez, Y. Karamanos, Targeting and crossing the blood-brain barrier with extracellular vesicles, Cells 9 (2020) 851.
[38] J.H. Kang, W.Y. Jang, Y.T. Ko, The effect of surface charges on the cellular uptake of liposomes investigated by live-cell imaging, Pharm. Res. (N. Y.) 34 (2017) 704–717.
[39] M. Kanamala, B.D. Palmer, S.M.F. Jamieson, W.R. Wilson, Z. Wu, Dual pH-sensitive liposomes with low pH-triggered sheddable PEG for enhanced tumor-targeted drug delivery, Nanomedicine 14 (2019) 1971–1989.
[40] J.N. Reginald-Opara, D. Svirskis, S.J. O'Carroll, S. Sreebhavan, J.M. Dean, Z. Wu, Optimisation of glutathione conjugation to liposomes quantified with a validated HPLC assay, Int. J. Pharm. 567 (2019) 118451.
[41] A.S. Jadli, N. Ballasy, P. Edalat, V.B. Patel, Inside (sight) of tiny communicator: exosome biogenesis, secretion, and uptake, Mol. Cell. Biochem. 467 (2020) 77–94.
[42] T. Yong, X. Zhang, N. Bie, H. Zhang, X. Zhang, F. Li, A. Hakeem, J. Hu, L. Gan, H.A. Santos, X. Yang, Tumor exosome-based nanoparticles are efficient drug carriers for chemotherapy, Nat. Commun. 10 (2019) 3838.
[43] H. Liu, M. Kang, J. Wang, C. Blenkiron, A. Lee, M. Wise, L. Chamley, Q. Chen, Estimation of the burden of human placental micro- and nano-vesicles extruded into the maternal blood from 8 to 12 weeks of gestation, Placenta 72–73 (2018) 41–47.
[44] A. Emelyanov, T. Shtam, R. Kamyshinsky, L. Garaeva, N. Verlov, I. Miliukhina, A. Kudrevatykh, G. Gavrilov, Y. Zabrodskaya, S. Pchelina, A. Konevega, Cryo-electron microscopy of extracellular vesicles from cerebrospinal fluid, PLoS One 15 (2020), e0227949.
[45] P. Cizmar, Y. Yuana, Detection and characterisation of extracellular vesicles by transmission and cryo-transmission electron microscopy, Methods Mol. Biol. 1660 (2017) 221–232.
[46] M.A.C. Pomatto, B. Bussolati, S. D'Antico, S. Ghiotto, C. Tetta, M.F. Brizzi, G. Camussi, Improved loading of plasma-derived extracellular vesicles to encapsulate antitumor mirnas, Mol. Ther. Methods Clin. Dev. 13 (2019) 133–144.
[47] J. Panyam, V. Labhasetwar, Dynamics of endocytosis and exocytosis of poly(D,L-Lactide-Co-glycolide) nanoparticles in vascular smooth muscle cells, Pharm. Res. (N. Y.) 20 (2003) 212–220.
[48] F. Illien, N. Rodriguez, M. Amoura, A. Joliot, M. Pallerla, S. Cribier, F. Burlina, S. Sagan, Quantitative fluorescence spectroscopy and flow cytometry analyses of cell-penetrating peptides internalization pathways: optimization, pitfalls, comparison with mass spectrometry quantification, Sci. Rep. 6 (2016) 36938.
[49] C.A. Bader, T. Shandala, Y.S. Ng, I.R.D. Johnson, D.A. Brooks, Atg9 is required for intraluminal vesicles in amphisomes and autolysosomes, Biol. Open 4 (2015) 1345–1355.
[50] S. Takahashi, K. Kubo, S. Waguri, A. Yabashi, H.W. Shin, Y. Katoh, K. Nakayama, Rab11 regulates exocytosis of recycling vesicles at the plasma membrane, J. Cell Sci. 125 (2012) 4049–4057.
[51] R. Villaseñor, M. Schilling, J. Sundaresan, Y. Lutz, L. Collin, Sorting tubules regulate blood-brain barrier transcytosis, Cell Rep. 21 (2017) 3256–3270.
[52] A. Patabendige, B.D. Michael, A.G. Craig, T. Solomon, Brain microvascular endothelial-astrocyte cell responses following Japanese encephalitis virus infection in an in vitro human blood-brain barrier model, Mol. Cell. Neurosci. 89 (2018) 60–70.
[53] A. Parr, I. J. Hidalgo, C. Bode, W. Brown, M. Yazdanian, M. A. Gonzalez, K. Sagawa, K. Miller, W. Jiang, E. S. Stippler. The Effect of Excipients on the Permeability of BCS.
[54] B. Dos Santos Rodrigues, H. Oue, A. Banerjee, T. Kanekiyo, J. Singh, Dual functionalized liposome-mediated gene delivery across triple co-culture blood brain barrier model and specific in vivo neuronal transfection, J. Contr. Release 286 (2018) 264–278.
[55] K.K. Huynh, S. Grinstein, Regulation of vacuolar pH and its modulation by some microbial species, Microbiol. Mol. Biol. Rev. 71 (2007) 452–462.
[56] P.E. Strømhaug, P.O. Seglen, Evidence for acidity of prelysosomal autophagic/endocytic vacuoles (amphisomes), Biochem. J. 291 (1993) 115–121.
[57] G. Maulucci, M. Chiarpotto, M. Papi, D. Samengo, G. Pani, M. De Spirito, Quantitative analysis of autophagic flux by confocal imaging of autophagic intermediates, Autophagy 11 (2015) 1905–1916.
[58] T.O. Berg, M. Fengsrud, P.E. Strømhaug, T. Berg, P.O. Seglen, Isolation and characterisation of rat liver amphisomes: evidence for fusion of autophagosomes with both early and late endosomes, J. Biol. Chem. 273 (1998) 21883–21892.
[59] S. Buratta, B. Tancini, K. Sagini, F. Delo, E. Chiaradia, L. Urbanelli, C. Emiliani, Lysosomal Exocytosis, Exosome release and secretory autophagy: the autophagic- and endo-lysosomal systems go extracellular, Int. J. Mol. Sci. 21 (2020) 2576.

[60] B. Hosseinkhani, S. Kuypers, van den Akker, M.S. Nynke, D.G.M. Molin, L. Michiels, Extracellular vesicles work as a functional inflammatory mediator between vascular endothelial cells and immune cells, Front. Immunol. 9 (2018) 1789.
[61] T. Zeng, X. Wang, W. Wang, Q. Feng, G. Lao, Y. Liang, C. Wang, J. Zhou, Y. Chen, J. Liu, H. Gao, B. Lan, Y. Wu, Y. Han, Y. Liu, H. Chen, L. Liu, C. Yang, L. Yan, M. Ren, K. Sun, Endothelial cell-derived small extracellular vesicles suppress cutaneous wound healing through regulating fibroblasts autophagy, Clin. Sci. 133 (2019), CS20190008.
[62] Y. Abdalla, M. Luo, E. Mäkilä, B.W. Day, N.H. Voelcker, W.Y. Tong, Effectiveness of porous silicon nanoparticle treatment at inhibiting the migration of a heterogeneous glioma cell population, J. Nanobiotechnol. 19 (2021) 60.
[63] H. Karanth, R.S. Murthy, pH-sensitive liposomes-principle and application in cancer therapy, J. Pharm. Pharmacol. 59 (2007) 469–483.
[64] S.J. Kuravi, C.M. Yates, M. Foster, P. Harrison, J. Hazeldine, P. Hampson, C. Watson, A. Belli, M. Midwinter, G.N. Nash, Changes in the pattern of plasma extracellular vesicles after severe trauma, PLoS One 12 (2017), e0183640.
[65] M. Maugeri, M. Nawaz, A. Papadimitriou, A. Angerfors, A. Camponeschi, M. Na, M. Hölttä, P. Skantze, S. Johansson, M. Sundqvist, J. Lindquist, T. Kjellman, I. Mårtensson, T. Jin, P. Sunnerhagen, S. Östman, L. Lindfors, H. Valadi, Linkage between endosomal escape of LNP-mRNA and loading into EVs for transport to other cells, Nat. Commun. 10 (2019) 4333.
[66] C.M. Fader, D. Sánchez, M. Furlán, M.I. Colombo, Induction of autophagy promotes fusion of multivesicular bodies with autophagic vacuoles in K562 cells, Traffic 9 (2008) 230–250.
[67] T. Worzfeld, M. Schwaninger, Apicobasal polarity of brain endothelial cells, J. Cerebr. Blood Flow Metabol. 36 (2016) 340–362.
[68] R. Daneman, A. Prat, The blood-brain barrier, Cold Spring Harbor Perspect. Biol. 7 (1) (2015) a020412.